Hindawi
International Journal of Chemical Engineering
Volume 2022, Article ID 8251430, 14 pages
https://doi.org/10.1155/2022/8251430

Research Article

Local Resistances of Gas–Liquid Two-Phase Flows in Vertical L-Shaped and Z-Shaped Pipes

Bing Wang,[1,2] Shan-qun Chen,[1,2] and Bin Liao[1,2]

[1]*College of Architecture and Civil Engineering, Anhui Polytechnic University, Anhui, Wuhu 241000, China*
[2]*Key Laboratory for Mechanics, Anhui Polytechnic University, Anhui, Wuhu 241000, China*

Correspondence should be addressed to Shan-qun Chen; chenshanqun@126.com

Received 23 August 2022; Revised 9 November 2022; Accepted 16 November 2022; Published 28 November 2022

Academic Editor: Junwu Wang

In this paper, a systematic numerical study of the local resistance coefficients of vertical L-shaped and Z-shaped pipes for gas–liquid two-phase flows under vertical conditions was carried out using a realizable k-ε turbulence model combined with a mixture model in Fluent software. Specifically, the influence of the Reynolds number Re_l, the gas-phase volume rate α, the radius–diameter ratio R/D, the height–diameter ratio H/D, and the two-phase flow direction on the local resistance coefficient ξ were discussed in detail. ξ of the vertical Z-shaped pipe decreases with increasing Re_l, while ξ of the vertical L-shaped pipe does not change significantly. In a specific range, ξ of vertical L-shaped and Z-shaped pipes increases with increasing α and decreases with increasing R/D. In Z-shaped pipes, under the upward flow condition, ξ increases with increasing H/D, and under the downward flow and horizontal flow conditions, ξ first decreases and then increases with increasing H/D. Overall, upward and downward flow conditions have a larger ξ than the horizontal flow condition. When H/D is larger than 14, ξ tends to be stable under all three flow conditions. Finally, the relationship equations between ξ and Re_l, α, R/D, and H/D were fitted, which agreed with the numerical results.

1. Introduction

Gas–liquid two-phase flow in a bend is a widespread flow phenomenon widely found in many engineering practices, including petroleum, chemical, natural gas, nuclear energy, aerospace, and other applications [1, 2]. When fluid flows through the bend, the combined effect of centrifugal force and wall pressure produces a gas–liquid two-phase flow with an extremely complex gas–liquid interface distribution and flow structure, such as reverse flow, overflow, and secondary flow [1]. Accordingly, these complex flow structures can also affect the flow state of inlet and outlet fluids, thus, causing a change in the fluid flow states and pressure pulsation in the pipe, which in turn induces coupled vibrations between the fluid and the pipe [3]. When the vibration frequency is the same as the inherent frequency of the pipe, a "resonance" phenomenon is produced [4], which is likely to cause pipe fatigue damage, especially in multibend components, and even cause damage to the piping system in severe cases, bringing substantial economic losses. The local resistance in the transit of a pipe is the additional loss over and above the friction resistance along the journey brought on by the presence of a bend. This additional loss extends beyond the bend's geometric length and affects the fluid's state upstream and downstream of the bend by a certain amount. Energy conservation and emission reduction are currently receiving a lot of attention across a variety of industries due to the increasing contradiction between energy demand and the ecological environment that has resulted from the social economy's rapid development. The amount of transportation energy used by a pipe system directly depends on the resistance value of the bend in a gas–liquid two-phase flow pipe. Therefore, studying the local resistances of gas–liquid two-phase flows in bends has significant academic value and extensive practical engineering significance.

For many years, the study of gas–liquid two-phase flows in bends has received widespread attention and has been the subject of extensive investigations by many scholars.

Statistically and inductively, the fluctuation of pressure in a bend is closely related to the variation in the gas–liquid two-phase flow pattern, which is often influenced by many factors such as the inner bend diameter, characterization of fluid flow velocity, fluid medium, and pipe arrangement [5–7]. The current gas–liquid two-phase flows in pipes are generally referenced according to the classification of flow patterns summarized in experiments by Baker [8] and Hewitt and Roberts [9]. Specifically, Baker classified the flow patterns occurring in horizontal straight pipes as bubble flow, plug flow, stratified flow, wavy flow, slug flow, and annular flow, while Hewitt and Roberts classified the flow patterns occurring in vertical straight pipes as bubble flow, slug flow, churn flow, annular flow, and wispy annular flow. Owing to the flow patterns mentioned above, the accurate prediction of the pressure drop in multiphase flow is often much more complex than in single-phase flow when predicting the pressure drop in bends. Therefore, most of the current prediction models for pressure drops in bends are based on single-phase flow. The more popular existing single-phase flow prediction models generally follow the Lockhart–Martinelli theory [10], which was originally proposed for vertical and horizontal straight pipes.

While this theory was mostly used to predict the pressure drop per unit length of a straight pipe for a single gas phase flow, scholars found that the theory also has high agreement for pressure loss calculations for a single liquid phase and gas–liquid mixture flow in pipes [11]. Later, a theoretical model proposed by Chisholm [12] significantly contributed to predicting the pressure drops of gas–liquid two-phase flows in bends. By discussing the pressure drop characteristics of gas–liquid two-phase flows in bends under horizontal conditions (without considering the effect of gravity), he proposed a prediction model based on two-phase multipliers. The model can be applied to frictional pressure drops, namely, local resistances of gas–liquid two-phase flows in bends with a wide range of radius–diameter ratios (as illustrated in Figure 1(a), which is an abbreviation for the curve radius of the bend to the diameter of the pipe), the diameters of the bends and different flow rates. Based on the Lockhart–Martinelli model and the Chisholm model, many modified pressure drop prediction models based on these two theoretical models have been proposed. Representative work includes the general relation between pressure drop characteristics and the Reynolds number proposed by Spedding and Benard [13] for an L-shaped pipe with a diameter of 26 mm and the pressure drop prediction relation for a U-shaped pipe with gas–liquid two-phase flow associated with the Chisholm model by Hayashi et al. [14]. The above studies both showed good correlations when compared with experimental data. Subsequent work has found that the pressure drops in bends change with the flow motion state and the geometry of the bend. A new T-junction pressure drop prediction model using a BP neural network (BPNN) was developed by Zhi et al. [15], which differs from the traditional prediction model based on theoretical analysis. Furthermore, the genetic algorithm (GA) and the particle swarm optimization (PSO) algorithm were combined with BPNN to optimize the weights and biases of BPNN. Correspondingly, scholars have examined the various relationships between the pressure drop and the flow condition or geometry of a bend. Saber and Maree [16] found that a significant pressure drop occurs at higher air flow rates through a numerical model constructed for a vertical L-shaped pipe.

Almabrok et al. [17] measured the pressure drop at diverse bend locations during upward and downward flow. It was found that the trends of the pressure gradient along the bend in different flow directions appear to be quite different, and the magnitude of the pressure gradient is also affected by the flow rate of each phase. Mazumder and Siddique [18] numerically studied the gas–liquid two-phase flow in a vertical bend with a diameter of 12.7 mm under three different gas and liquid phase velocity conditions. It was found that the gas–liquid two-phase flow showed a significant pressure drop as it left the bend, and the pressure drop was also more significant at higher gas flow velocities.

In summary, much research has been done by scholars on the pressure drops of gas–liquid two-phase flows in bends. However, most of these studies were still based on a horizontal condition, while less research has considered the effect of gravity. Moreover, even less work has been done to study the local resistances of gas–liquid two-phase flows in bends.

Although gas–liquid two-phase flow in a vertical bend is a common phenomenon in many engineering practices, the local resistances of gas–liquid two-phase flows in vertical bends under the effect of gravity have not yet been investigated in depth. Hence, systematic numerical research is conducted here for the local resistances of vertical gas–liquid two-phase flows in bends under the effect of gravity. Specifically, a three-dimensional numerical model of gas–liquid two-phase flows in vertical L-shaped and Z-shaped pipes is constructed, and the applicability and accuracy of the numerical model are validated. The effects of dimensionless parameters such as the radius–diameter ratio, height–diameter ratio (as illustrated in Figure 1(b), which is an abbreviation for the height between the bends to the diameter of the pipe), Reynolds number, and gas-phase volume rate of the gas–liquid two-phase flow on the variation in the flow field structure are systematically investigated. Furthermore, the influences of the geometric characteristics and flow conditions of vertical L-shaped and Z-shaped pipes on the local resistance are studied in detail. Finally, the relationship equations between the local resistance coefficients of vertical L-shaped and Z-shaped pipes and the above dimensionless parameters are numerically fitted. This study can enrich our understanding of the local resistances of gas–liquid two-phase flows in bends.

2. Numerical Model and Calculation of the Local Resistance Coefficient

2.1. Governing Equations. Here, an mixture model based on the commercial computational fluid dynamics (CFD) software Fluent was selected to numerically simulate the gas–liquid two-phase flow in the bends. A mixture model is a simplified multiphase flow model based on the Euler–Euler

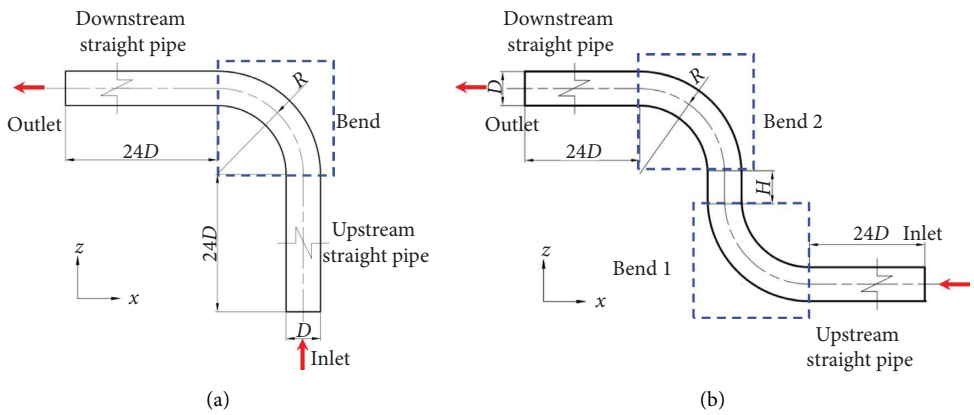

Figure 1: Side view of the pipe 3D calculation domain. (a) L-shaped pipe, (b) Z-shaped pipe. The red arrows denote the direction of the incoming and outgoing flows at the inlet and outlet, respectively.

method, which can be used for uniform multiphase flow without the relative velocity of discrete phases. Specifically, the multiphase flow was simulated by solving the continuity, momentum, and energy equations.

The governing equations are specified as follows:

Continuity equation:

$$\frac{\partial}{\partial t}(\rho) + \nabla \cdot (\rho \cdot \mathbf{v}) = 0, \tag{1}$$

where $\boldsymbol{v}$ is the mean velocity of the gas–liquid two-phase flow, ρ is the mean density of the gas–liquid two-phase phase flow, $\rho = \sum_{i=1}^{n} \alpha_i \rho_i$, n is the number of phases, α_i is the volume fraction of phase i, and ρ_i is the density of phase i.

Momentum equation:

$$\frac{\partial}{\partial t}(\rho \cdot \mathbf{v}) + \nabla \cdot (\rho \cdot \mathbf{v}) = -\nabla p + \nabla \cdot \left[\mu\left(\nabla \mathbf{v} + \nabla \mathbf{v}^T\right)\right] + \rho \mathbf{g} + \mathbf{F} - \nabla \cdot \left(\sum_{i=1}^{n} \alpha_i \rho_i \mathbf{v}_{\text{move}}\right), \tag{2}$$

where p is the pressure, $\mathbf{F}$ is the body force, μ is the mean viscosity of the gas–liquid two-phase flow, $\mu = \sum_{i=1}^{n} \alpha_i \mu_i$, μ_i is the viscosity of phase i, $_{\text{move}}$ is the slip velocity of phase i, $\mathbf{v}_{\text{move}} = \mathbf{v}_i - \mathbf{v}$, is the velocity of phase i, and is the mean velocity of the gas–liquid two-phase flow.

Energy equation:

$$\frac{\partial}{\partial t}\sum_{i=1}^{n}(\alpha_i \rho_i W_i) + \nabla \cdot \sum_{i=1}^{n}(\alpha_i \mathbf{v}_i(\rho_i W_i + P)) = \nabla \cdot \left(\omega_{eff}\nabla T - \sum_{i}\sum_{j} C_{j,i}\boldsymbol{\varphi}_{j,i} + \left(\omega_{eff} \cdot \mathbf{v}\right)\right) + S_\omega, \tag{3}$$

where W_i is the energy of phase i, T is the temperature, $C_{j,\,i}$ is the enthalpy of phase j in phase i, $\boldsymbol{\varphi}_{j,\,i}$ is the diffusion flux of phase j in phase i, ω_{eff} is the effective thermal conductivity of the gas–liquid two-phase flow, $\omega_{eff} = \sum_{i=1}^{n} \alpha_i(\omega_i + \omega_t)$, ω_i is the thermal conductivity of phase i, ω_t is the turbulent thermal conductivity defined according to the turbulence model, and S_ω is the source item.

2.2. Realizable k-ε Turbulence Model. Owing to the combined effects of gravity, buoyancy, and centrifugal force, the gas–liquid two-phase flow in a vertical bend is prone to generating complex flows, such as secondary flow and overflow. The realizable k-ε turbulence model is considered to have significant advantages in solving complex structures with rapidly changing flow velocities [19]. Accordingly, the realizable k-ε turbulence model was selected here to

numerically simulate the flow structure of the gas–liquid two-phase flow in a vertical bend.

The turbulent kinetic energy k and turbulent energy dissipation rate ε in the realizable k-ε turbulence model can be solved by the following equations:

$$\frac{\partial(\rho k)}{\partial t}+\frac{\partial(\rho k u_j)}{\partial x_j}=\frac{\partial}{\partial x_j}\left[\left(\mu+\frac{\mu_t}{\sigma_k}\right)\cdot\frac{\partial k}{\partial x_j}\right]+G_k-\rho\varepsilon,$$
$$\frac{\partial(\rho \varepsilon)}{\partial t}+\frac{\partial(\rho \varepsilon u_j)}{\partial x_j}=\frac{\partial}{\partial x_j}\left[\left(\mu+\frac{\mu_t}{\sigma_\varepsilon}\right)\cdot\frac{\partial \varepsilon}{\partial x_j}\right]+\rho C_1 S\varepsilon-\rho C_2\frac{\varepsilon^2}{k+\sqrt{v\varepsilon}}, \tag{4}$$

where x_j is the coordinate component, u_j is the mean relative velocity component, G_k is the generation item of turbulent kinetic energy, μ_t is the turbulent viscosity coefficient, v is the dynamic viscosity, and C_1, C_2, σ_k, and σ_ε are all the model constants. The experience values of the model constants are $C_1 = \max[0.43, (\zeta/\zeta+5)]$ (where $\zeta = S(k/\varepsilon)$, $S=\sqrt{2S_{ij}S_{ij}}$, $S_{ij}=(1/2)((\partial u_i/\partial x_j)+(\partial u_j/\partial x_i))$, $C_2 = 1.9$, $\sigma_k = 1.0$, and $\sigma_\varepsilon = 1.2$).

2.3. Computational Domain. The side views of the 3D vertical pipe calculation domain are shown in Figure 1, which consists of an upstream straight pipe, an 90° bend, and a downstream straight pipe. The longitudinal profile along the central axis is located in the XZ plane, and the direction of gravity is set to the negative direction of the Z-axis. As illustrated in Figure 1, D is the diameter of the bend, $D = 30$ mm, and R is the bend's curvature radius. The Z-shaped pipe is a combination of two L-shaped pipes. H is the height between the two L-shaped pipes. It should be noted that D remains constant in all the numerical simulations. Accordingly, the dimensionless parameters R/D and H/D, which are the expressions of the radius–diameter ratio and height–diameter ratio, respectively, can be used to distinguish the pipe geometries under different R and H conditions. Specifically, $R/D = 1$ to 7 and $H/D = 1$ to 15 were selected to analyze the local resistance of the pipe under different geometric conditions. In addition, considering the full development of upstream and downstream flow when entering and leaving the bend, the upstream and downstream straight pipe lengths are both taken as 24 D.

For the gas–liquid two-phase flow in the bend in this paper, water and air were selected as the liquid and gas phases, respectively. The liquid phase is selected as the primary phase, while the gas phase is selected as the second one. The velocity inlet condition was adopted at the inlet of the pipe to maintain the exact velocity of both gas–liquid phases. To achieve a wide range of Reynolds number conditions, we set the velocity range as = 1 to 10 m/s, with the direction perpendicular to the inlet. In addition, the outflow boundary condition was adopted at the outlet, and no-slip boundaries were adopted on all the walls.

2.4. Calculation of the Local Resistance Coefficient. The local resistance of the gas–liquid two-phase flow in the vertical bend under gravity was measured by the local resistance coefficient ξ, which was calculated as follows:

$$\Delta p=\xi\frac{\rho v^2}{2}, \tag{5}$$

where Δp is the local resistance, which can be expressed by

$$\Delta p=\Delta p_{\text{total}}-\Delta p_{\text{geod}}-\Delta p_{\text{loss}}, \tag{6}$$

where Δp_{total} is the total pressure drop at the bend, Δp_{geod} is the change in gravitational potential energy generated when the fluid flows through the bend, $\Delta p_{\text{geod}} = \rho g h$ (where h is the height difference when the fluid flows through the bend), and Δp_{loss} is the along-travel pressure drop when the fluid flows through the bend, $\Delta P_{\text{loss}} = \varphi(l/D)\cdot(\rho v^2/2)$, where φ is a coefficient of the along-travel pressure drop, $\varphi = (0.3164/Re^{0.25})$. It should be noted that according to equation (5), Δp can be considered to be in line with the trend of ξ when the mean density and velocity of the gas–liquid two-phase flow do not change.

Moreover, to further achieve dimensionless conditions, the liquid phase Reynolds number Re_l was selected to distinguish the effect of fluid velocity on Δp, which is expressed as

$$\text{Re}_l=\frac{\rho_l v_l D}{v_l}, \tag{7}$$

where ρ_l, v_l, and v_l are the density, velocity, and kinematic viscosity of the liquid phase, respectively.

2.5. Meshing and Grid-Independence Validation. Schematic diagrams of calculation domain meshing are shown in Figure 2. As illustrated in Figure 2, the computational domains have meshed with a structural hexahedral mesh. Stress concentration is likely to occur at the bend, which in turn forms a reverse flow region and makes the flow more complicated. Therefore, the grid at the bend is locally refined. Moreover, it is well known that the quality and quantity of meshing can significantly impact a numerical simulation and directly affect the speed and accuracy of the numerical results. To optimize the computational efficiency based on the available hardware, grid-independence validation was performed. Specifically, numerical models with grid numbers of 540,000, 710,000, 910,000, and 1,180,000 were selected to calculate the gas–liquid two-phase flows in

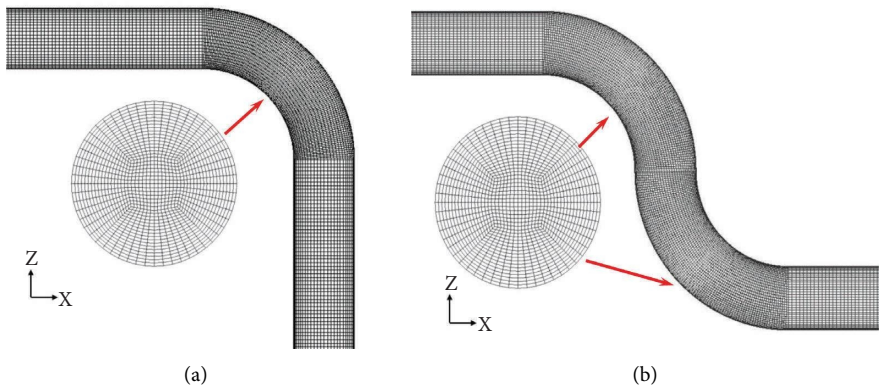

Figure 2: Schematic diagrams of calculation domain meshing. (a) L-shaped pipe, (b) Z-shaped pipe.

vertical L-shaped pipes, and numerical models with grid numbers of 1,010,000, 1,310,000, 1,700,000, and 2,210,000 were used to calculate the gas–liquid two-phase flows in vertical Z-shaped pipes. The grid-independence validation results, ξ, under different grid number conditions are listed in Table 1. It should be noted that we measured how closely the results of the simulations aligned with the most refined case as a benchmark, i.e., the cases with grid numbers of 1,180,000 and 2,210,000 for vertical L-shaped pipe and Z-shaped pipe, respectively. Hence, we defined the error η of the difference between cases with other grid numbers and the maximum grid number case to be

$$\eta = \left|\frac{\xi_i - \xi_m}{\xi_m}\right|, \tag{8}$$

where ξ_m is the local resistance coefficient of the cases with the maximum grid number and ξ_i is the local resistance coefficient of the cases with other grid numbers.

It was found that η of the L-shaped pipe with 540,000 grid numbers is greater than 50% compared to the other two cases, while η of the L-shaped pipe with 710,000 grid numbers is less than 11% of the numerical models with larger grid numbers. Moreover, η of the L-shaped pipe with 710,000 grid numbers is very close to that of the L-shaped pipe with 910,000 grid numbers. Similarly, η of the Z-shaped pipe with 1010,000 grid numbers is greater than 5% compared to the other two cases, while η of the Z-shaped pipe with 1310,000 grid numbers is less than 1% of the numerical models with larger grid numbers. Finally, the numerical models with grid numbers 710,000 and 1,310,000 were selected to simulate the gas–liquid two-phase flows in vertical L-shaped and Z-shaped pipes, respectively. It should be noted that H/D was set to 0 in Figure 2(b) for the grid-independence validation. In the subsequent simulations when H/D is not equal to 0, the grid numbers of vertical Z-shaped pipes will increase accordingly.

2.6. Calculation Verification of Local Resistance. Referring to the experimental data conducted by Azzi and Friedel [20] on the local resistances of the gas–liquid two-phase flows in vertical L-shaped pipes, we selected six identical cases for comparison with their experimental data. The specific parameters of different gas volume fractions α and Re_l are listed in Table 2. The comparison of numerical results and experimental data is illustrated in Figure 3. Δp_{exp} indicates the local resistance obtained experimentally by Azzi and Friedel [20], and Δp_{num} indicates the local resistance calculated by numerical simulation. Each point in Figure 4 represents an experimental or numerical result. In addition, we fitted the numerical results and added an error range of ±10% to visualize the difference between the numerical results and experimental data. It was found that the experimental data are all within the ±10% error of the fitted line of the numerical results. Accordingly, it can be concluded that the numerical model adopted here has good applicability and high accuracy for studying the local resistances of vertical gas–liquid two-phase flows in vertical bends.

3. Local Resistance Characteristics and Corresponding Influencing Factors

3.1. Local Resistance Characteristics. It is generally accepted that in gas–liquid two-phase flow, the energy dissipation and momentum exchange between the two phases caused by the separation and mixing phenomena occurring in the gas and liquid phases is an essential reason for the increase in local resistance in the bend [21]. Specifically, when the fluid flows through the bend, centrifugal force is generated this moves from the momentum center of the bend to the outer wall. The centrifugal force interacts with the boundary layer when the fluid adheres to the wall. Correspondingly, two identical vortices are formed, as shown in Figure 4. These are the main reasons for the formation of secondary flow when the gas–liquid two-phase flow passes through the bend.

Subsequently, to reveal the effect of the bend on the pressure distribution of the gas–liquid two-phase flows in the pipe, the pressure distribution curve along the horizontal L-shaped and Z-shaped pipe from the inlet to the outlet is extracted, as shown in Figures 5(a) and 6(a), respectively. It should be noted that the numerical conditions of this case are $R/D = 2$, $\alpha = 0.15$ and $Re_l = 59713$, $H/D = 4$ in Z-shaped pipes. In addition, L is the length along the whole pipe. The horizontal coordinate 0 indicates the position where the

Table 1: Results of grid-independence validation.

Type of pipes	Grid numbers	ξ	η	Type of pipes	Grid numbers	ξ	η
L-shaped	540,000	0.129	0.743	Z-shaped	1010,000	0.448	0.069
L-shaped	710,000	0.066	0.108	Z-shaped	1310,000	0.481	0
L-shaped	910,000	0.068	0.081	Z-shaped	1700,000	0.478	0.006
L-shaped	1180,000	0.074	—	Z-shaped	2210,000	0.481	—

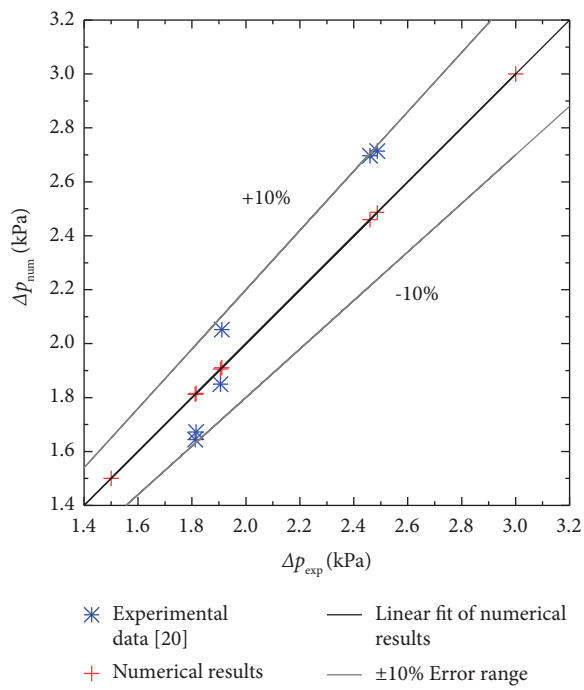

Figure 3: Comparison of numerical results and experimental data [20].

Table 2: Numerical conditions under different α and Re_l corresponding to Azzi and Friedel [20].

Cases of [20]	α	Re_l
A	0	39848
B	0.331	59563
C	0.592	97676
D	0.71	137434
E	0.826	229067
F	0.905	419513

center of the pipe axis is located, and the coordinate of the upstream section of the pipe is negative while the downstream is positive. Moreover, to investigate the pressure distribution characteristic in detail, the curve of pressure change rate k along the pipe are illustrated in Figures 5(b) and 6(b), respectively, where the positive value indicates an increase in pressure and the negative value indicates a decrease in pressure. Based on these two figures, it was found that k is almost constant upstream of the pipe. Namely, the pressure drop of the gas–liquid two-phase flow shows an almost constant trend since the flow is hardly disturbed before flowing through the bend. Subsequently, it was found that k changes drastically at the bend compared to the upstream of

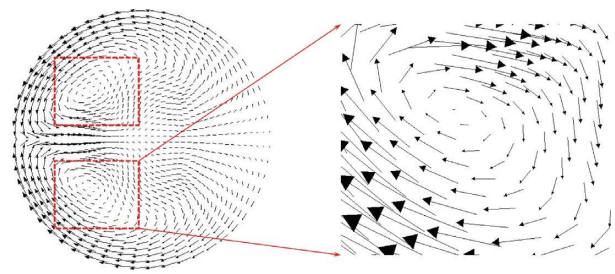

Figure 4: Velocity vector distribution of the cross-section at the bend. The red dashed boxes indicate the region where vortices are formed.

the pipe. The pressure drop takes a significant upward turn at the bend. Referring to the analysis results in reference [22], the main reason for that is the disturbance effect of the secondary flow near the bend. Moreover, this disturbance effect is more evident in the short distance upstream and downstream of the pipe, and the influence distance in the downstream direction is more prolonged than in the upstream direction. Therefore, the two bends (as illustrated in Figure 1(b), which are bends 1 and 2, respectively) of the Z-shaped pipe interact with each other, showing a slightly different trend of k. Specifically, k at bend 2 is slightly greater than at bend 1. Finally, owing to the weakening of the disturbance effect caused by the bend, the k in the downstream of the pipe also shows an almost constant trend. Notably, the k values in the upstream and downstream of the pipe are almost the same. The above analysis results show that the local resistance of the gas–liquid two-phase flow bend has prominently different characteristics compared to the straight pipes.

3.2. Influencing Factors for Local Resistance. It is generally accepted that gravity in nonhorizontal flow conditions can significantly affect the local resistance. Specifically, the shear stress is constantly changing under the effect of gravity, resulting in different shear stress distributions in different flow planes. However, referring to reference [20], the pressure loss due to this mechanism is negligible concerning the local pressure loss. Accordingly, scholars generally agree that the main reason for the significant effect of gravity on the local resistance is the combined effect of gravity and centrifugal force at the bend. In this case, very complex flow phenomena will occur at the vertical bends, such as the mixing of gas and liquid phases and the inversion of the flow, which will give the vertical, bend a relatively higher local resistance than the horizontal bend.

The different motion states of the gas and liquid phases produce different flow patterns at the bend, resulting in changes in the local resistance. Specifically, the gas and liquid

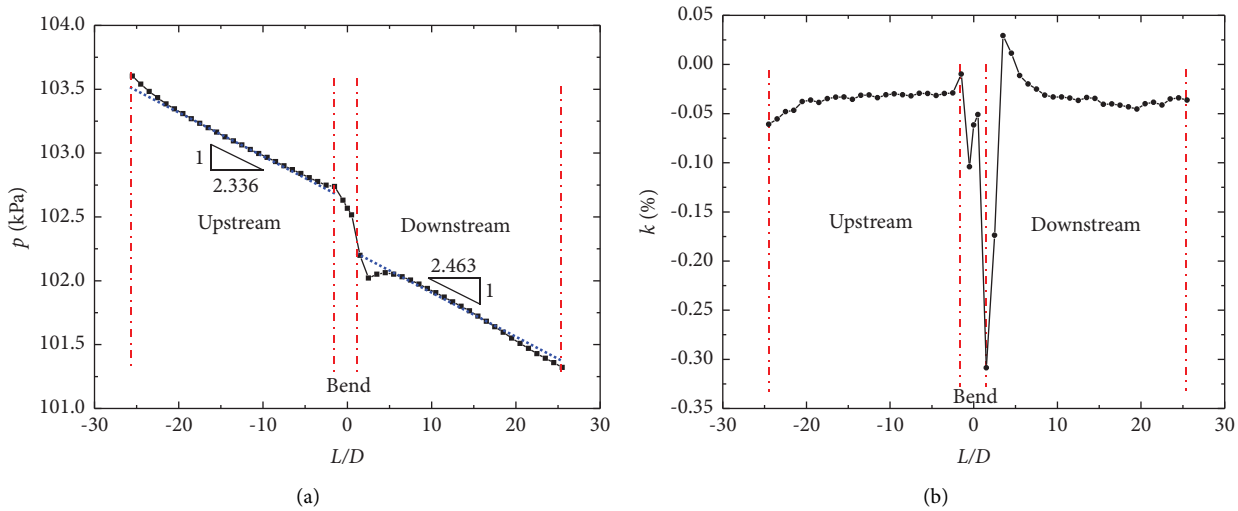

Figure 5: Pressure distribution characteristic curve along the horizontal L-shaped pipe: (a) Pressure distribution curves along the pipe from the inlet to the outlet, (b) The change rate of pressure along the pipe from the inlet to the outlet.

phases can flow either on the outside or inside at the bend, depending mainly on the balance between the centrifugal force that pushes the liquid phase to the outside and the gravity that forces it to the inside. This equilibrium relationship can be expressed in terms of the Froude number Fr_θ, which can be written as follows:

$$Fr_\theta = \frac{v^2}{gR\sin\theta}, \tag{9}$$

where v is the mean velocity of the gas–liquid phases and θ is the bending angle of the bend. It is generally accepted that when $Fr_\theta = 1$, the gas–liquid two-phase flow equilibrium is in the radial direction of the bend. Furthermore, when $Fr_\theta > 1$, the gas phase moves to the inside of the bend and the liquid phase moves to the outside of the bend. Finally, when $Fr_\theta < 1$ is reached, the two-phases move in the opposite direction to the former condition.

Moreover, when studying the local resistance of multiphase flow in the bend, the wall roughness and the surface tension are generally excluded as influencing factors because their effects are much smaller than the inertial force [23]. Therefore, combining the analysis results above, the local resistance of the gas–liquid two-phase flow mainly depends on the density of each phase, the geometry of the bend, and gravity [24]. Correspondingly, the main influencing factors on the local resistance discussed in this study are, α, R/D, H/D, and gravity.

4. Results and Discussion for L-Shaped Pipes

4.1. Effect of Re_l and α on the Local Resistance. According to the local resistance calculated by equation (5), when the change in ξ is neglected, the local resistance of the bend is proportional to v^2 and decreases with increasing α. In this case, we first used a dimensionless parameter called the local resistance ratio λ to verify the relationships between ξ, α, and Re_l. The expression of λ is written as follows:

$$\lambda = \frac{\Delta p}{\Delta p_r}, \tag{10}$$

where Δp_r is the local resistance of the vertical L-shaped pipe at $R/D = 2$, $\alpha = 0$, and $Re_l = 89569$. Then, the relationship curves of λ with different α and Re_l are shown in Figure 7. It should be noted that R/D was equal to 2 in all of these cases. It was found that λ increases with increasing Re_l, which is consistent with equation (5). The main reason for this is that the increase in the flow rate increases the frictional shear between the fluid and the bend wall and the shear at the interface between the gas and liquid phases [25]. In addition, the secondary flow velocity at the bend also increases, increasing the local resistance. Finally, it was also found that the local resistance increases when α increases from 0.1 to 0.2 and significantly decreases when it increases from 0.2 to 0.3. The above analysis results are a significant departure from what is expressed in equation (5) above, which suggests that ξ is affected when Re_l and α are changed.

The relationship curves of ξ with Re_l under different α in the vertical L-shaped pipe are shown in Figure 8. R/D was also equal to 2 in all of these simulations. It was found that the relationship curves of Re_l versus ξ do not vary much, i.e., the effect of the flow velocity in the bend on ξ is small. In other words, the increase in secondary flow velocity is the main reason for the increase in local resistance at the bend. Moreover, ξ increases continuously with increasing α, and the rising trend decreases with increasing Re_l. Specifically, ξ significantly changes when α increases from 0 to 0.2, after which it can be approximated that the change in ξ is independent of α. The main reason for that is that, compared to the single-phase flow, gas–liquid two-phase flow contains more complex flow states, such as a mixture between gas–liquid phases and inversion of gas–liquid two-phase flow. In this case, more momentum is exchanged between the gas and liquid phases in the bend when α increases and the increasing trend decreases with the increase in α in a specific range.

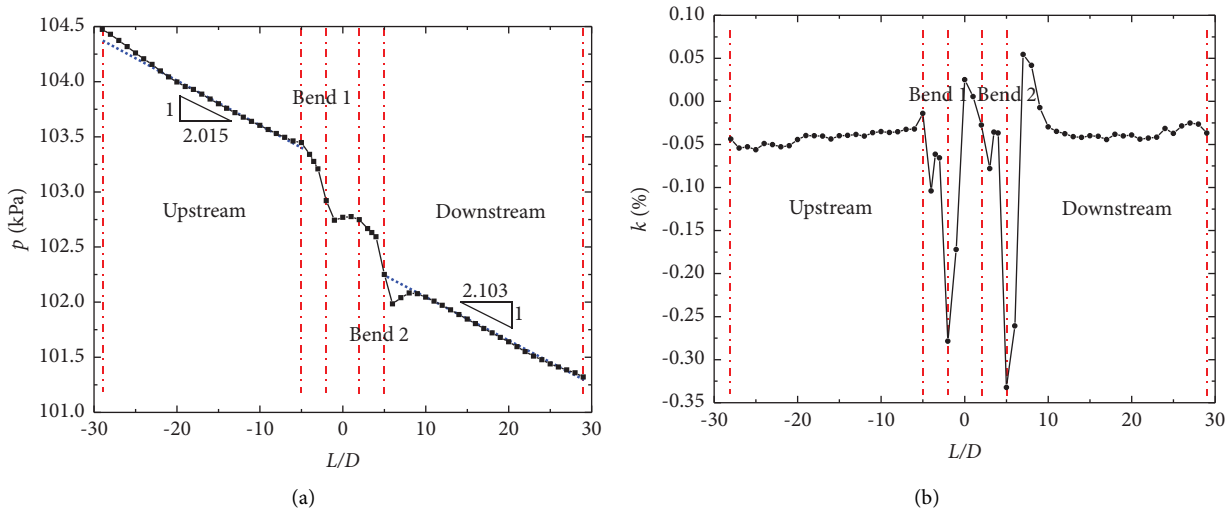

Figure 6: Pressure distribution characteristic curves along the horizontal Z-shaped pipe. (a) Pressure distribution curves along the pipe from the inlet to the outlet and (b) the change rate of pressure along the pipe from the inlet to the outlet.

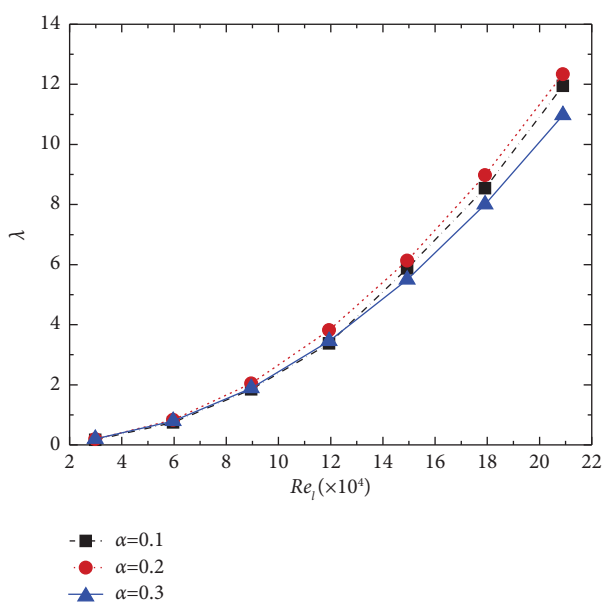

Figure 7: Relationship curves of λ with Rel under different α in vertical L-shaped pipes.

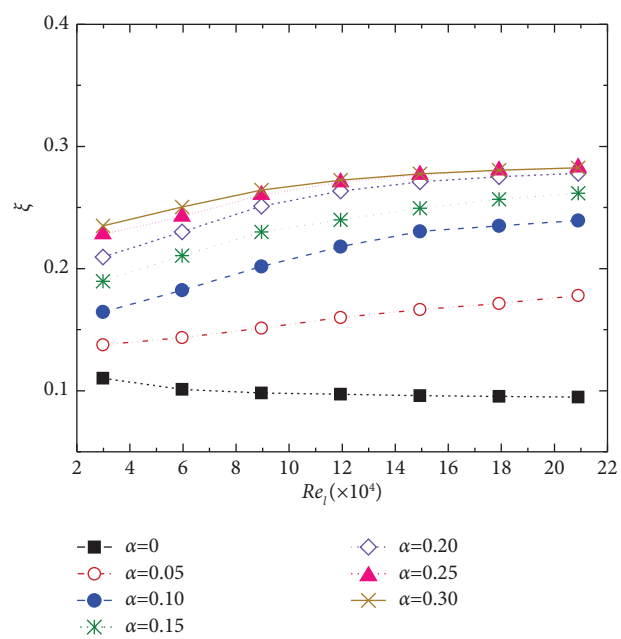

Figure 8: Relationship curves of ξ with Re_l under different α in vertical L-shaped pipes.

4.2. Effect of R/D on the Local Resistance. The relationship curves of ξ with R/D under different Re_l in the vertical L-shaped pipe are illustrated in Figure 9. It should be noted that α was equal to 0.15 in all cases. It was found that the curves for different Re_l values have almost the same trend. In addition, when $R/D > 5$, the curves overlap. The above analysis results are consistent with the previous statement that Re_l does not show much effect on ξ. Furthermore, in Figure 9, it was also found that ξ decreases at first and then stabilizes as R/D increases. Specifically, ξ decreases rapidly as R/D increases from 1 to 2. The reason for this is that under relatively small R/D conditions, the strong inertial and centrifugal forces generate reverse flow near the bend, which is shown in Figure 10. Accordingly, the reverse flow region increases the dissipation of energy into the gas–liquid two-phase flow and has a significant impact on the local resistance of the bend. Subsequently, as R/D continues to increase, the centrifugal force at the bend decreases due to the increase in the curvature radius. Meanwhile, the gas–liquid two-phase flow in the bend has a relatively greater development region, accompanied by a decrease in the secondary flow velocity, which decreases the reverse flow region near the bend significantly until it disappears. In this case, the effect of R/D on ξ gradually decreases until $R/D > 5$, ξ is almost unchanged.

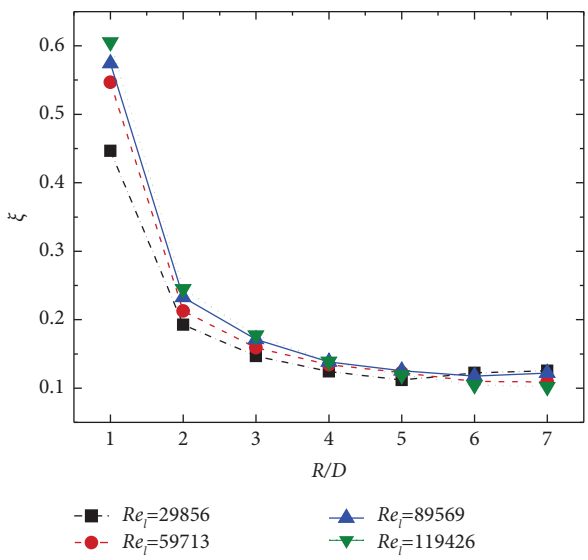

Figure 9: Relationship curves of ξ with R/D under different Re_l in vertical L-shaped pipes.

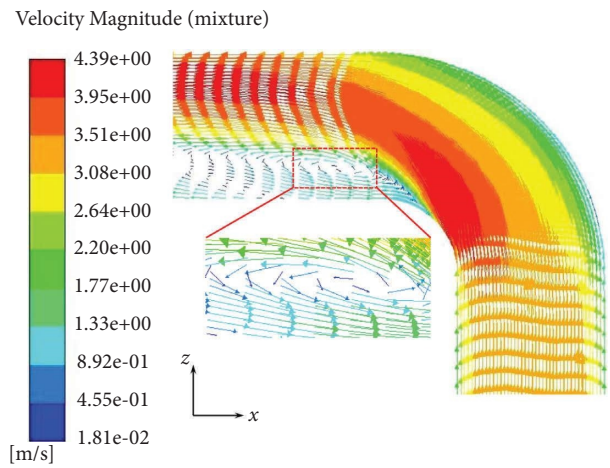

Figure 10: Generation of reverse flow near the bend in a vertical L-shaped pipe. The red dashed box represents the reverse flow region.

5. Results and Discussion for Z-Shaped Pipes

5.1. Effect of R/D and α on the Local Resistance. The relationship curves of ξ with R/D under different α in vertical Z-shaped pipes are illustrated in Figure 11. It should be noted that Re_l and H/D were all equal to 89569 and 1 in these cases, respectively. ξ increases as α increases, and the increasing trend of α from 0.05 to 0.15 is more significant than that from 0.15 to 0.25. It was also found that when R/D increases from 1 to 8, ξ decreases continuously, and the ξ - R/D curves gradually flatten out. Until $R/D > 5$, the curves are parallel to the horizontal axis. This indicates that the effect of R/D on local resistance is minimal when $R/D > 5$ and can be ignored. This result is consistent with the conclusion exhibited by L-shaped pipes when varying R/D and α.

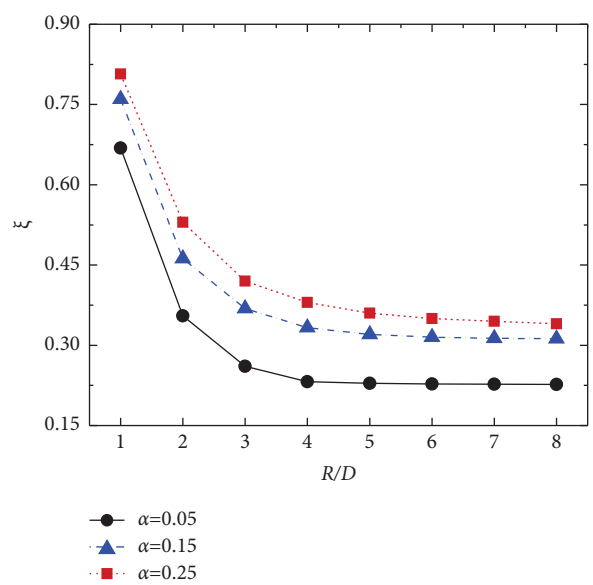

Figure 11: Relationship curves of ξ with R/D under different α in vertical Z-shaped pipes.

5.2. Effect of Flow Direction on the Local Resistance. Compared with vertical L-shaped pipes, gas–liquid two-phase flows in vertical Z-shaped pipes have more complex flow states. Since the flow states of gas–liquid two-phase flows in different flow directions are very different, it is necessary to investigate the effect of different flow directions on the local resistance. Correspondingly, Figure 12 illustrates the relationship curves of ξ with Re_l under three different flow directions in Z-shaped pipes. It should be noted that the upward flow direction is the same as the red arrow denoted in Figure 1(b), the downward flow direction is the opposite of the upward flow direction, and the horizontal flow direction represents the flow direction in a horizontal Z-shaped pipe. In addition, R/D, H/D, and α were equal to 2, 1, and 0.15 in these cases, respectively. The overall trend of the curves decreases, then gradually flattens out, and finally converges to a constant value. Specifically, when Re_l is relatively small, as Re_l increases, the turbulent fluctuation of the gas–liquid two-phase flow in the bend is enhanced, and the turbulent kinetic energy is also exchanged vigorously, causing strong anisotropy in the flow field and weakening the effect of secondary flow on ξ [26]. While Re_l is relatively large, namely, $Re_l > 10^5$, there is a minor change in ξ. The reason for that is the flow in the bend entering the squared resistance region, the variation in ξ is usually considered independent of Re_l at this moment.

It was also found that the effect of Re_l on the local resistance in the horizontal bend is significantly smaller than that in the vertical bend. We consider the main reason for that to be the effect of centrifugal force. Specifically, centrifugal force affects the fluids in the bend, which causes both the liquid and gas phases to flow toward the outer wall in the horizontal condition. However, since two-phase flows have a more significant proportion of liquid phase than gases, and the liquid phase's mass is greater than the gas phase, liquids possess a much greater centrifugal force than gases. Thus, during the outward flow of liquid, the gas is constantly pushed against the inner wall of the bend. Compared to the

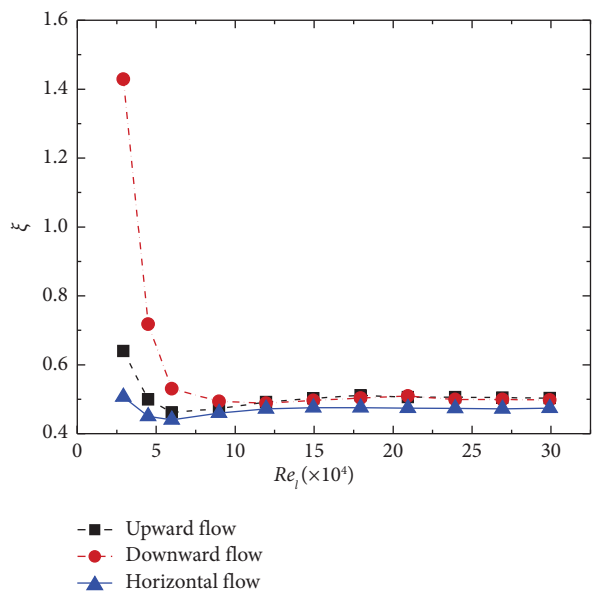

Figure 12: Relationship curves of ξ with Re_l under three different flow directions in Z-shaped pipes.

horizontal condition, the fluids in the bend will also be affected by gravity in the vertical condition. In such a condition, the gas phase can move inward or outward around the bend, depending on the balance between centrifugal force and gravity [20].

On the other hand, due to the Re_l being closely related to the two-phase flow velocity, the centrifugal force changes as the two-phase flow velocity changes. Besides, the fluid state in the bend may significantly change as the centrifugal force and gravity in a vertical bend generally act together. Therefore, the influence of Re_l in the vertical condition is more significant than in the horizontal condition, and the local resistance of the former is more significant than that of the latter under buoyancy.

Moreover, the different flow directions in the vertical bend impose a specific difference on the local resistance due to the role of buoyancy. Specifically, when the flow velocity of gas–liquid two-phase flow is low, the two-phase fluid in the bend behaves as a plug-bubble flow with alternating long gas plugs and liquid columns [27]. The buoyancy effect of long gas plugs and large bubbles has a more significant obstructive effect on the downward flow direction of the gas–liquid two-phase flow. This obstructive effect makes ξ in downward flow much larger than ξ in upward flow. Finally, when the flow velocity increases, the length and diameter of the bubble in the bend decrease. Meanwhile, the obstructive effect on the downward flow is also gradually reducing. In this case, ξ for different flow directions in the vertical bend is almost the same.

5.3. Effect of H/D on the Local Resistance. Since the main body of the Z-shaped pipe is a combination of two L-shaped pipes, its local resistance is bound to be influenced by the spacing H between the two L-shaped pipes. Therefore, it is necessary to investigate the effect of H/D on the local resistance. Correspondingly, Figure 13 illustrates the relationship curves of ξ with H/D under three different flow directions in Z-shaped pipes. It should be noted that R/D, Re_l, and α were equal to 2, 89569, and 0.15 in these cases, respectively. It was found that when H/D increases to 14, ξ of the Z-shaped pipe converges to a constant value, which is approximately equal to the two times ξ of the L-shaped pipe under the same numerical parameters. This analysis result indicates that the interaction between the two L-shaped pipes no longer occurs when $H/D > 14$.

Moreover, in the horizontal and downward flow conditions, ξ first shows a trend of decreasing and increasing with increasing H/D. This is because under relatively small H/D conditions, the reverse flow region of the first bend does not have time to expand into the second bend, and the reverse flow is not fully developed, resulting in local pressure loss in the bend. As H/D increases, the reverse flow region develops wholly and gradually, causing ξ to decrease. In the upward flow condition, unlike the above two flow conditions, ξ continues to increase with increasing H/D. The reason is that the buoyancy effect brought by the giant bubbles promotes the two-phase flow with an upward flow, resulting in ξ not showing a descending trend.

Finally, when $H/D > 4$, ξ under the three flow directions shows an increasing trend. The influence between the two bends will lead to secondary flow in the middle straight pipe section. The larger H/D *is*, the greater the pressure loss caused by secondary flow, so ξ increases with increasing H/D. Until H reaches the maximum influence length (H is approximately 14 D in this study), the two bends no longer affect each other. Hence, two independent bends were formed. In this case, ξ does not change when $H/D > 14$.

6. Approximate Fitting of the Local Resistance Coefficient

6.1. Vertical L-Shaped Pipe. According to the above analysis results, ξ of the vertical L-shaped pipe is closely related to Re_l, α, and R/D. Referring to Cai et al. [28] for the form of pressure drop prediction relation of L-shaped pipe, a relationship equation can be established between ξ and the above parameters, which is expressed as follows:

$$\xi = M \cdot Re_l^A \cdot \alpha^B \cdot \left(\frac{R}{D}\right)^C + N, \tag{11}$$

where M, N, A, B, and C are all constants.

The variables in equation (11) take the following values: $Re_l = 2.9 \times 10^4 \sim 21.0 \times 10^4$, $\alpha = 0 \sim 0.3$, and $R/D = 1 \sim 7$. The numerical simulation data were fitted to obtain the values of five constants, M, N, A, B, and C, as listed in Table 3.

The final equation for the relationship between ξ and the above parameters is as follows:

$$\xi = \frac{0.00473 Re_l^{0.431} \cdot \alpha^{0.245}}{(R/D)^2} + 0.118. \tag{12}$$

The values of ξ predicted by equation (12) were compared with those from the numerical simulation, which is shown in Figure 14. Each point represents a numerical result. In

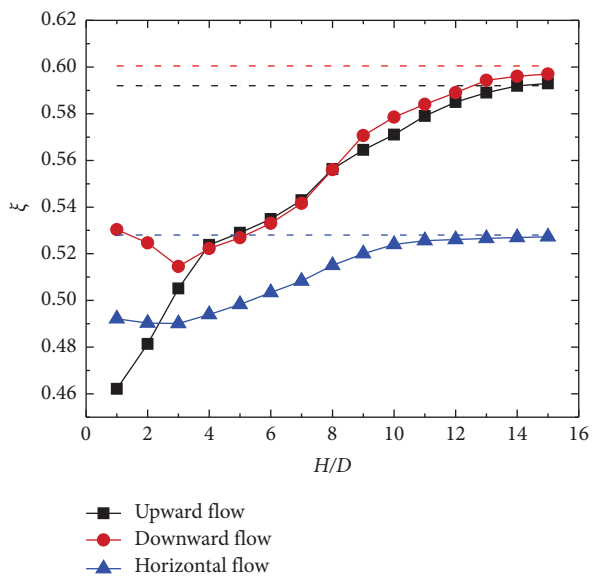

Figure 13: Relationship curves of ξ with H/D under three different flow directions in Z-shaped pipes. Horizontal dashed lines indicate two times ξ of the L-shaped pipes under the same numerical parameters.

Table 3: The values of the constants in equation (12).

M	N	A	B	C
0.00473	0.118	0.431	0.245	−2

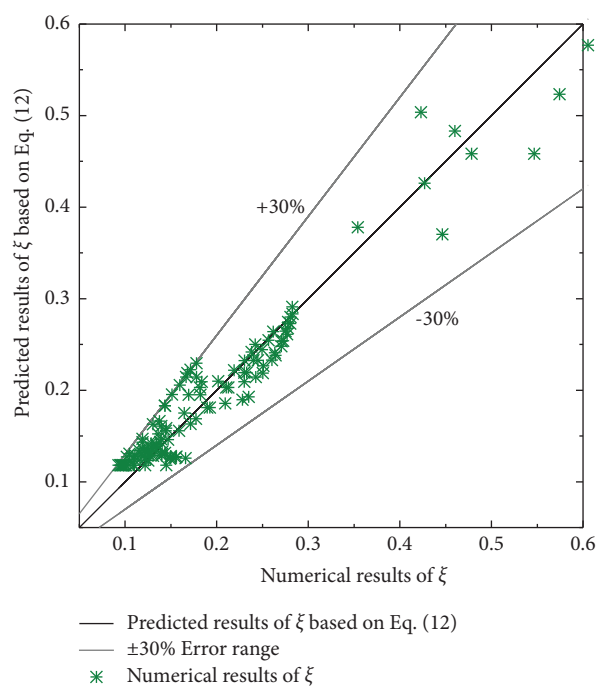

Figure 14: Comparison of predicted and numerical results of ξ in vertical L-shaped pipes.

addition, we added an error range of ±30% to visualize the difference between the predicted results based on equation (12) and numerical results. It was found that the numerical results are all within ±30% error of the predicted results based on equation (12). Accordingly, it can be concluded that equation (12) can predict ξ of a vertical L-shaped pipe accurately.

Table 4: The values of the constants under different flow directions in equation (13).

Directions	a	b	c	d
Upward	0.013	−0.575	0.089	0.269
Downward	−0.455	−0.591	−0.090	−2.657

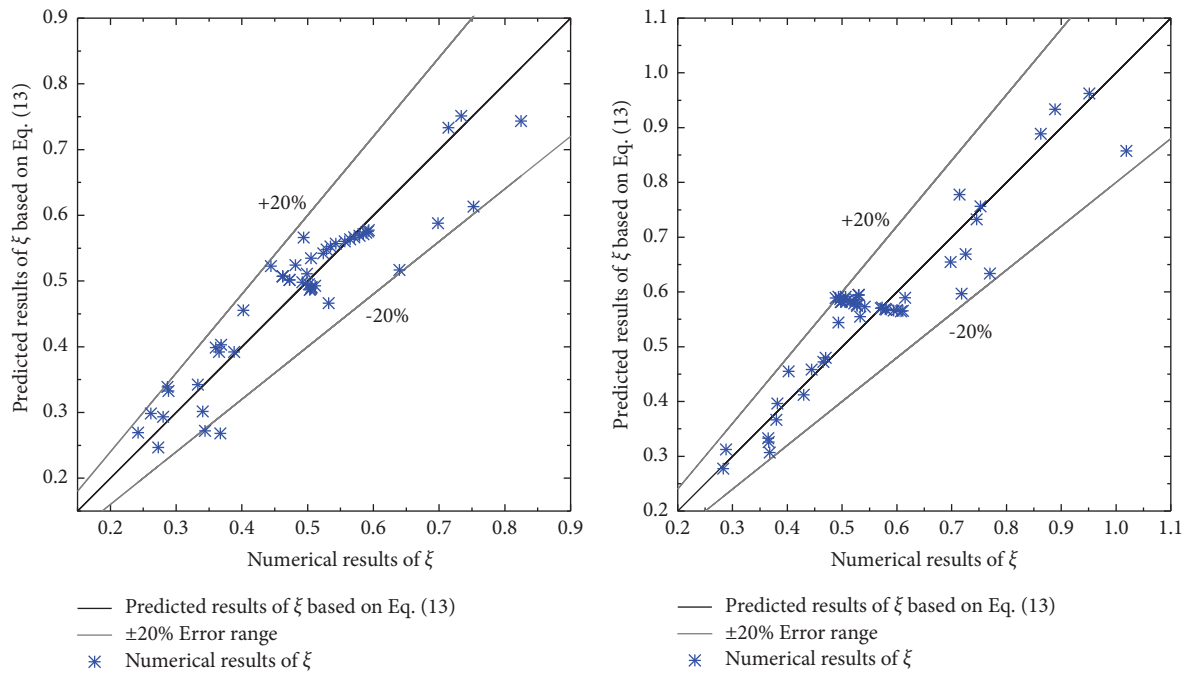

Figure 15: Comparison of predicted and numerical results of ξ in vertical Z-shaped pipes. (a) Upward flow and (b) downward flow.

6.2. Vertical Z-Shaped Pipe. Similar to the vertical L-shaped pipe, ξ of the vertical L-shaped pipe is closely related to Re_l, α, R/D, and H/D. Referring to Chen et al. [29] for the form of pressure drop prediction relation of U-shaped pipe, a relationship equation can also be established between ξ and the above parameters of the Z-shaped pipe, which is expressed as follows:

$$\xi = Re_l^a \cdot \left(\frac{R}{D}\right)^b \cdot \left(\frac{H}{D}\right)^c \cdot \alpha^d, \tag{13}$$

where a, b, c, and d are all constants.

The variables in equation (13) take the following values: $Re_l = 2.9 \times 10^4 \sim 30.0 \times 10^4$, $R/D = 1\sim7$, $H/D = 1\sim15$, and $\alpha = 0\sim0.3$. The numerical simulation data under two different flow conditions were fitted to obtain the values of four constants, a, b, c, and d, as listed in Table 4.

The values of ξ predicted by equation (13) were compared with those from the numerical simulation, which is shown in Figure 15. Each point represents a numerical result. In addition, we added an error range of ±20% to visualize the difference between the predicted results based on equation (13) and numerical results. It was found that the numerical results under two different flow directions are all within ±30% error of the predicted results based on equation (13). Accordingly, it can be concluded that equation (13) can accurately predict ξ of the vertical Z-shaped pipe under two different flow directions.

7. Concluding Remarks

A three-dimensional numerical model of gas–liquid two-phase flow in vertical L-shaped and Z-shaped pipes was constructed, and related experimental data validated the applicability and accuracy of the numerical model. Based on this, the effects of dimensionless parameters such as R/D, H/D, Re_l, and α on the variation of the flow field structure were systematically investigated. Furthermore, the influences of the geometric characteristics and flow conditions of vertical L-shaped and Z-shaped pipes on the local resistance were studied in detail. Finally, the relationship equations between ξ of vertical L-shaped and Z-shaped pipes and R/D, H/D, Re_l, and α were fitted. The following conclusions can be drawn.

(1) Re_l fewer influences ξ for vertical L-shaped pipes, and the local resistance is proportional to the square of Re_l on the whole based on remaining the other parameters constant.

(2) Under a relatively small Re_l, ξ decreases as Re_l increases in the vertical Z-shaped pipe, when Re_l continues to increase, ξ will not significantly differ in value. The vertical bend has a larger ξ than the horizontal bend due to the combined effect of centrifugal force and gravity. The buoyancy effect of

large bubbles makes ξ of downward flow much higher than that of upward flow under a relatively small Re_l.

(3) Under the upward flow condition, ξ of the vertical Z-shaped pipe increases as H/D increases. Under horizontal and vertical downward flow conditions, ξ first decreases and then increases with increasing H/D. However, in all three flow directions, ξ remains unchanged after the distance between the two bends reaches a maximum influence length of 14 D.

(4) The CFD results in L-shaped and Z-shaped pipes both showed a similar trend and behavior for the same flow conditions with slight differences in values, and both with increasing R/D expressed a trend of first decreasing and then basically unchanged. The effects of these factors are minor and no longer sufficient to cause significant variation in ξ at $R/D > 5$. Within a specific range, a raising α leads to an increase in flow reversal and energy dissipation, resulting in an improving ξ of gas–liquid two-phase flow in the bends.

(5) The relationship equations between ξ and dimensionless parameters, i.e., Re_l, α, R/D, and H/D, were obtained based on numerical fitting. It was found that the errors between the predicted and numerical results in vertical L-shaped and Z-shaped pipes are less than 30% and 20%, respectively.

Data Availability

The data that support the findings of this study are available from the corresponding author upon reasonable request.

Conflicts of Interest

The authors declare that they have no conflicts of interest.

Acknowledgments

The work described in this paper is sponsored by The Anhui Provincial Natural Science Foundation (2008085QA22), The Preresearch Project of the National Science Foundation of Anhui Polytechnic University (Xjky2020167), The Science and Technology Planning Project of Wuhu City, Anhui Province (2021jc1-2), The Domestic Visiting Program for Outstanding Young Teachers in High Institutions of Anhui Province (gxgnfx2022013), and The Scientific Research Project for the Graduate Student in High Institutions of Anhui Province (YJS20210454).

References

[1] M. Vatani and D. Domiri-Ganji, "Experimental examination of gas–liquid two-phase flow patterns in an inclined rectangular channel with 90 bend for various vertical lengths," *International Journal of Engineering*, vol. 35, no. 4, pp. 685–691, 2022.

[2] S. Qiao and S. Kim, "On the prediction of two-phase pressure drop across 90° vertical elbows," *International Journal of Multiphase Flow*, vol. 109, pp. 242–258, 2018.

[3] L. Wang, Y. Yang, Y. Li, and Y. Wang, "Resonance analyses of a pipeline-riser system conveying gas–liquid two-phase flow with flow-pattern evolution," *International Journal of Pressure Vessels and Piping*, vol. 161, pp. 22–32, 2018.

[4] S. Miwa, T. Hibiki, and M. Mori, "Analysis of flow-induced vibration due to stratified wavy two-phase flow," *Journal of Fluids Engineering*, vol. 138, no. 9, 2016.

[5] X. Ma, M. Tian, J. Zhang, L. Tang, and F. Liu, "Flow pattern identification for two-phase flow in a U-bend and its contiguous straight tubes," *Experimental Thermal and Fluid Science*, vol. 93, pp. 218–234, 2018.

[6] R. Zahedi and A. Babaee Rad, "Numerical and experimental simulation of gas-liquid two-phase flow in 90-degree elbow," *Alexandria Engineering Journal*, vol. 61, no. 3, pp. 2536–2550, 2022.

[7] P. Amani, S. Hurter, V. Rudolph, and M. Firouzi, "Comparison of flow dynamics of air–water flows with foam flows in vertical pipes," *Experimental Thermal and Fluid Science*, vol. 119, Article ID 110216, 2020.

[8] O. Baker, "Design of pipelines for the simultaneous flow of oil and gas," in *Proceedings of the Fall Meeting Of The Petroleum Branch of AIME*, Dallas, TX, USA, October 1953.

[9] G. F. Hewitt and D. N. Roberts, *Studies of Two-phase Flow Patterns by Simultaneous X-ray and Flash Photography (No. AERE-M-2159)*, Atomic Energy Research Establishment, Harwell, England, 1969.

[10] R. W. Lockhart, "Proposed correlation of data for isothermal two-phase, two-component flow in pipes," *Chemical Engineering Progress*, vol. 45, pp. 39–48, 1949.

[11] D. Chisholm, "A theoretical basis for the Lockhart-Martinelli correlation for two-phase flow," *International Journal of Heat and Mass Transfer*, vol. 10, no. 12, pp. 1767–1778, 1967.

[12] D. Chisholm, "Two-phase flow in heat exchangers and pipelines," *Heat Transfer Engineering*, vol. 6, no. 2, pp. 48–57, 1985.

[13] P. L. Spedding and E. Bénard, "Gas–liquid two phase flow through a vertical 90° elbow bend," *Experimental Thermal and Fluid Science*, vol. 31, no. 7, pp. 761–769, 2007.

[14] K. Hayashi, J. Kazi, N. Yoshida, and A. Tomiyama, "Pressure drops of air–water two-phase flows in horizontal U-bends," *International Journal of Multiphase Flow*, vol. 131, Article ID 103403, 2020.

[15] C. S. Zhi, Y. X. Zhang, C. Zhu, and Y. W. Liu, "Numerical analysis and artificial neural network-based prediction of two-phase flow pressure drop of refrigerants in T-junction," *International Journal of Refrigeration*, vol. 137, pp. 34–42, 2022.

[16] H. A. Saber and I. E. Maree, "A computational study of curvature effect on pressure drop of gas-liquid two-phase flow through 90 degree elbow," *Thermal Science*, vol. 26, no. 4 Part A, pp. 3215–3228, 2022.

[17] A. A. Almabrok, A. M. Aliyu, Y. D. Baba et al., "A comparative analysis of upward and downward pressure gradient behaviour in vertical gas–liquid two-phase flows in a large diameter pipe facility," in *Proceedings of the SPE Nigeria Annual International Conference and Exhibition*, Lagos, Nigeria, August 2020.

[18] Q. H. Mazumder and S. A. Siddique, "CFD analysis of two-phase flow characteristics in a 90 degree elbow," *The Journal of Computational Multiphase Flows*, vol. 3, no. 3, pp. 165–175, 2011.

[19] Z. W. Wang, Y. P. He, M. Z. Li et al., "Fluid–structure interaction of two-phase flow passing through 90° pipe bend under slug pattern conditions," *China Ocean Engineering*, vol. 35, no. 6, pp. 914–923, 2021.

[20] A. Azzi and L. Friedel, "Two-phase upward flow 90 bend pressure loss model," *Forschung im Ingenieurwesen*, vol. 69, no. 2, pp. 120–130, 2005.

[21] B. A. Shannak, "Frictional pressure drop of gas liquid two-phase flow in pipes," *Nuclear Engineering and Design*, vol. 238, no. 12, pp. 3277–3284, 2008.

[22] N. M. Tripathi, D. Portnikov, A. Levy, and H. Kalman, "Bend pressure drop in horizontal and vertical dilute phase pneumatic conveying systems," *Chemical Engineering Science*, vol. 209, Article ID 115228, 2019.

[23] A. M. Aliyu, Y. D. Baba, L. Lao, H. Yeung, and K. C. Kim, "Interfacial friction in upward annular gas–liquid two-phase flow in pipes," *Experimental Thermal and Fluid Science*, vol. 84, pp. 90–109, 2017.

[24] M. Ghobadi and Y. S. Muzychka, "A review of heat transfer and pressure drop correlations for laminar flow in curved circular ducts," *Heat Transfer Engineering*, vol. 37, no. 10, pp. 815–839, 2016.

[25] P. O. Ayegba, L. C. Edomwonyi-Otu, A. Abubakar, and N. Yusuf, "Flow pattern and pressure drop for oil–water flows in and around 180° bends," *SN Applied Sciences*, vol. 3, no. 1, pp. 10–13, 2021.

[26] J. Li, J. H. Yang, T. Huang, K. Han, and L. Gao, "Numerically studying effects of Reynolds number and radius ratio on flow characteristics of 90° arc bend pipe," *Mechanical Science and Technology for Aerospace Engineering*, vol. 36, no. 10, pp. 1491–1497, 2017, (in Chinese).

[27] C. C. Wang, I. Y. Chen, Y. W. Yang, and Y. J. Chang, "Two-phase flow pattern in small diameter tubes with the presence of horizontal return bend," *International Journal of Heat and Mass Transfer*, vol. 46, no. 16, pp. 2975–2981, 2003.

[28] L. Cai, S. Liu, X. Pan et al., "Comparison of pressure drops through different bends in dense-phase pneumatic conveying system at high pressure," *Experimental Thermal and Fluid Science*, vol. 57, pp. 11–19, 2014.

[29] I. Y. Chen, C. L. Won, and C. C. Wang, "Influence of oil on R-410A two-phase frictional pressure drop in a small U-type wavy tube," *International Communications in Heat and Mass Transfer*, vol. 32, no. 6, pp. 797–808, 2005.